iTRAQ-based quantitative proteome analysis reveals metabolic changes between a cleistogamous wheat mutant and its wild-type wheat

Caiguo Tang [1,2,†], Huilan Zhang [1,2,†], Pingping Zhang [3], Yuhan Ma [1], Minghui Cao [1,2], Hao Hu [1,2], Faheem Afzal Shah [1], Weiwei Zhao [1], Minghao Li [1,2,*] and Lifang Wu [1,*]

[1] Key laboratory of high magnetic field and Ion beam physical biology, Hefei Institutes of Physical Science, Chinese Academy of Sciences, Hefei, Anhui, China;

[2] School of Life Sciences, University of Science and Technology of China, Hefei, Anhui, China

[3] School of Life Sciences, Anhui University, Hefei, Anhui, China

[†] These authors contributed equally to this work.

*Corresponding Author:

Minghao Li; Lifang Wu

350 Shushanhu Road, Hefei 230031, Anhui, P. R. China

Email address: limh@ipp.ac.cn (M.L); lfwu@ipp.ac.cn (L.W)

Abstract

Background: Wheat is one of the most important staple crops worldwide. *Fusarium* head blight severely affects wheat yield and quality. A novel bread wheat mutant, *ZK001*, characterised as cleistogamic was isolated from a non-cleistogamous variety (YM18) through static magnetic field mutagenesis. Cleistogamy is a promising strategy for controlling *Fusarium* head blight. However, little is known about the mechanism of cleistogamy in wheat.

Methods: We performed a *Fusarium* head blight resistance test to identify the *Fusarium* head blight infection rate of *ZK001*. We also measured the agronomic traits of *ZK001* and the starch and total soluble sugar contents of lodicules in YM18 and *ZK001*. Finally, we performed comparative studies at the proteome level between YM18 and *ZK001* based on the proteomic technique of isobaric tags for relative and absolute quantification.

Results: The infection rate of *ZK001* was lower than that of its wild type and AK58. The abnormal lodicules of *ZK001* lost the ability to push the lemma and palea apart during the flowering stage. Proteome analysis showed that the main differentially abundant proteins were related to carbohydrate metabolism, protein transport, and calcium ion binding. These differentially abundant proteins may work together to regulate cellular homeostasis, osmotic pressure and the development of lodicules. This hypothesis is supported by the analysis of starch, soluble sugar content in the lodicules as well as the results of qRT-PCR.

39 **Conclusions:** Proteomic analysis has provided comprehensive information that should be useful
40 for further research on the lodicule development mechanism in wheat. The *ZK001* mutant is
41 optimal for studying flower development in wheat and could be very important for *Fusarium* head
42 blight resistant projects via conventional crossing.
43

Introduction

45 Bread wheat (*Triticum aestivum* L.) is one of the most important staple crops worldwide. The
46 world population continues to grow and arable area is decreasing year by year, therefore higher
47 production in crop plants may prove to be necessary to satisfy the increasing demand for food
48 (FAO, 2015). However, many challenges, inclding biotic and abiotic stresses, severely affect
49 wheat fields and product quality. For instance, *Fusarium* head blight (FHB) is critically damaging
50 wheat security (Walter, Nicholson & Doohan, 2010), and the application of chemical insecticides
51 and fungicides is increasing the amounts of residues in wheat and in the environment
52 (Hollingsworth et al., 2008). Therefore, scientists and breeders have to find eco-friendly and cost-
53 effective strategies to guarantee wheat yield and quality..
54   In the last decade, severe epidemics caused by *Fusarium* spp. have occurred worldwide with
55 up to 100% yield loss recorded under optimal disease conditions (Yumurtaci et al., 2017). The
56 *pore-forming toxin-like* (*PFT*) gene at the quantitative trait locus (QTL) *Fhb1,* which was the first
57 FHB-resistance gene isolated, was found to confer resistance to FHB in Sumai 3 (SM3) (Rawat et
58 al., 2016). FHB infection usually occurs on the inner surfaces of lemmas and paleae after
59 germination of the *Fusarium* spp. conidia (Zange, Kang & Buchenauer, 2005). The anther can
60 provide the initial path for FHB infection (Pugh, Johann & Dickson, 1933; Walter, Nicholson &
61 Doohan, 2010); therefore, cleistogamous cultivars, which contain few anthers exposed to glumes,
62 may provide structural barriers for diseases that appear during the flowering stage. In barley
63 (*Hordeum vulgare* L.), cleistogamous cultivars, which self-fertilize within permanently closed
64 flowers (Culley & Klooster, 2007), showed greater resistance to FHB infection than
65 chasmogamous cultivars, which have open flowers (Yoshida, Kawada & Tohnooka, 2005). In
66 wheat, cleistogamous cultivars such as U24 have a lower risk of FHB infection than
67 chasmogamous cultivars such as Saikai 165 (Kubo et al., 2010). Therefore, cleistogamy might be
68 the basis for new strategies for controlling *Fusarium* head blight in cereal crops.
69   Cleistogamy in barley is genetically determined by the presence of the recessive allele *cly1*,
70 but the dominant allele at the linked locus, *Cly2*, is epistatic over *cly1* (Wang et al., 2013). Loss of
71 the miRNA172 target site causes *cly1* to express a protein, *Hv*AP2, which effectively suppresses
72 lodicule swelling (Turuspekov et al., 2004; Nair et al., 2010; Wang et al., 2015). In rice (*Oryza
73 sativa* L.), there are many cleistogamous mutants resulting from abnormal lodicules. A single
74 recessive gene, *lodiculeless spikelet(t)* [*ld(t)*], controls the cleistogamous mutant lacking lodicules
75 (Won & Koh, 1998; Maeng et al., 2006). Another rice mutant, which has a truncated DEP2
76 determined by the *cl7(t)* gene, has a cleistogamous phenotype because of weak swelling ability in
77 the lodicules (Ni et al., 2014). A third rice mutant, *spw1-cls*, has normal stamens, but the lodicules
78 are transformed homeotically into lodicule-glume mosaic organs, thereby engendering

79 cleistogamy with temperature-sensitivity (Yoshida et al., 2007; Ohmori et al., 2012). A novel
80 temperature-stable cleistogamous mutant, *spw1-cls2*, can maintain the cleistogamous phenotype
81 under low temperatures (Lombardo et al., 2017). The glumes open in the flowering stage because
82 the swelling of the lodicule is primarily responsible for pushing the lemma and palea, thereby
83 opening the floret (Nair et al., 2010). In contrast, there is very little information on cleistogamy in
84 wheat.

85   The probability of primary infection is approximately proportional to the number of spores
86 reaching the open florets during the flowering process; accordingly, the breeding of varieties with
87 flowers that are partially or completely cleistogamous might reduce *Fusarium* susceptibility in
88 wheat (Schuster & Ellner, 2008). In order to probe the mechanism of cleistogamy, Ning et al. (
89 2013) studied the structure, transcription and post-transcriptional regulation of the cleistogamous
90 gene *TaAP2*, which is homologous in barley and wheat. *TaAP2* alleles may also generate a
91 cleistogamous wheat and improve resistance to FHB. Additionally, anther extrusion is a complex
92 trait with significant markers; it has either favourable or unfavorable additive effects and imparts
93 minor to moderate levels of phenotypic variance in spring and winter wheat (Muqaddasi et al.,
94 2017).

95   Large-scale transcriptomic analyses have been employed in wheat to better understand the
96 molecular mechanisms of flower development (Winfield et al., 2010; Diallo et al., 2014; Feng et
97 al., 2015; Kumar et al., 2015; Yang et al., 2015; Ma et al., 2017). However, because of post-
98 transcriptional and post-translational modifications, mRNA levels do not always correlate with the
99 corresponding protein levels (Schweppe et al., 2003; Canovas et al., 2004; Zhao et al., 2013).
100 Proteins are directly correlated with cellular functions (Yan et al., 2005; Zhang et al., 2012);
101 therefore, proteomic analysis is essential for studying global protein expression levels in wheat to
102 further unravel the complex mechanisms of cleistogamy. In particular, isobaric tags for relative
103 and absolute quantitation (iTRAQ) technology, which is a quantitative gel-free proteomic
104 approach, coupled with liquid chromatography-tandem mass spectrometry (LC-MS/MS) enables
105 the direct quantification and comparison of protein levels among samples with more efficiency
106 and accuracy than traditional gel-based techniques which fail to identify low-abundance protein
107 species and have limitations for identifying proteins with extreme biochemical properties (Wu et
108 al., 2006).

109   Here, we show that an SMFs-induced wheat mutant, *ZK001*, is a cleistogamous line with
110 lower FHB infection vulnerability than the chasmogamous line Yumai 18 (YM18). Additionally,
111 we performed a comparative proteomic analysis of different development stages in YM18 and
112 *ZK001* to characterise the protein expression profiles. In this manner, we aimed to provide insight
113 into proteomic changes associated with the cleistogamous phenotype in wheat, specifically
114 exploring lodicule expanding mechanisms at the protein level. Our results have the potential to
115 benefit future research efforts in controlling FHB via conventional breeding, advance the study of
116 wheat flower development, and contribute to better control of genetically modified lines of
117 agriculturally important crops; this could lead to time and cost-savings in the effort to refine
118 genotypes.

119 **Materials & Methods**

120 **Plant Material**

121 The cleistogamy mutant line *ZK001*, was isolated from a mutagenised population of wheat variety
122 YM18, using an SMFs of 7 Tesla for 5 hours. After mutagenesis, it propagated via self-pollination
123 until the cleistogamous phenotype was completely stable. All wheat seeds were stored at the Hefei
124 Institutes of Physical Science, Chinese Academy of Sciences (CASHIPS), Anhui, P. R. China.
125 SM3, Aikang 58 (AK58), YM18 and *ZK001* were grown in a greenhouse in an experimental field
126 (31°54′ N, 117°10′ E) at CASHIPS. AK58 and YM18, which are both varieties in the northern
127 China, were not resistant to FHB infection (Yu et al., 2019). Therefore, AK58 was used as
128 susceptible control. Fertilizer and weed management were similar to methods used in the process
129 for wheat breeding (Li et al., 2014). The spikelets and lodicules of YM18 and *ZK001*, which had
130 three biological replicates, were harvested during the white anther stage (WAS), green anther stage
131 (GAS), yellow anther stage (YAS), and anthesis stage (AS) (Zadoks, Chang & Konzak, 1974;
132 Kirby & Appleyard, 1987; Guo & Schnurbusch, 2015). These samples were collected and frozen
133 in liquid nitrogen and preserved at -80 °C.

134 **Starch and total soluble sugar content**

135 Twenty pairs of lodicules with three biological replications from YM18 and *ZK001* were sampled
136 and snap frozen in liquid nitrogen at the four flower development stages. The samples were ground
137 using Tissuelyser-24 (Shanghai Jingxin Industrial Development Co., Ltd.) for 45 seconds at 50
138 Hz.

139 Starch and total soluble sugars were extracted following the instructions included with the Starch
140 Content and Plant Soluble Sugar Content test kits (Nanjing Jiancheng Bioengineering Institute).
141 The starch and total soluble sugars in the supernatant were determined using a UV-VIS
142 spectrophotometer (Lambda 365, PerkinElmer) with a wavelength of 620 nm. The starch and total
143 soluble sugar contents were calculated using the following formulas:

144

145
$$C_{starch} = \frac{OD_{sample} - OD_{blank}}{OD_{standard} - OD_{blank}} \times \frac{C_{standard\ 1} \times V_{pretreatment} \times \text{Dilution ratio}}{N_{total\ PL}}$$

146

147
$$C_{total\ souble\ sugar} = \frac{OD_{sample} - OD_{blank}}{OD_{standard} - OD_{blank}} \times \frac{C_{standard\ 2} \times \text{Dilution ratio}}{10 \times V_{distilled\ water} \times N_{total\ PL}}$$

148

149 Note: PL: pair of lodicules, C_{starch}: the starch content in lodicule ($\mu g \cdot PL^{-1}$), $C_{total\ souble\ sugar}$: the total
150 souble sugar content in lodicule ($\mu g \cdot PL^{-1}$), $C_{standard\ 1}$: standard solution 1 concentration = 200
151 $\mu g \cdot mL^{-1}$, $C_{standard\ 2}$: standard solution 2 concentration = 100 $\mu g \cdot mL^{-1}$, Dilution ratio = 1, $V_{pretreatment}$:

152   the volume of pretreatment solution = 1.7 mL, $V_{distilled\ water}$: the volume of distilled water used for
153   homogenising = 1 mL, $N_{total\ PL}$: the total number of PL which were sampled = 20.
154
155   **Observation of spikes and lodicules**
156   Spike images of YM18 and *ZK001* were photographed (D90, Nikon) at the AS. After 90 minutes,
157   the lodicules of YM18 and *ZK001*, which were separated from the central young spikes in triplicate
158   during GAS and cultured on Murashige and Skoog (MS) medium, were observed with an upright
159   fluorescence stereomicroscope (SZX10, Olympus) and photographed (DP72, Olympus).
160   **FHB resistance testing**
161   FHB resistance testing was performed during the flowering stage of SM3, AK58, YM18 and
162   *ZK001* in the greenhouse by spraying the FHB spore F0601 (*Fusarium graminearum* Schw. cv.
163   F0601) in both 2013-2014 and 2014-2015. The inoculum (50 μL at 105 spores per mL) was
164   deposited by spraying both sides of the ears. The diseased spikelet rate was calculated using the
165   following formula:
166
167     $$\text{Diseased spikelets rate} = \frac{N_{infected\ spikelets}}{N_{total\ spikelets}} \times 100\%.$$
168
169   Note: $N_{infected\ spikelets}$: the number of infected spikelets, $N_{total\ spikelets}$: the number of total spikelets.
170
171   **Protein extraction and iTRAQ labelling**
172   Total soluble proteins were extracted according to a published procedure (Yang et al., 2013) with
173   slight modifications. Briefly, moderate amounts of the samples were separately frozen using liquid
174   N_2 and ground in -20 °C pre-cooled pestles and mortars with urea extraction buffer containing 150
175   mM Tris-HCl (pH 7.6), 8 M urea, 0.5% SDS, 1.2% Triton X-100, 20 mM EDTA, 20 mM EGTA,
176   50 mM NaF, 1% glycerol 2-phosphate, 5 mM DTT, and 0.5% phosphatase inhibitor mixture 2
177   (Sigma). The mixtures were centrifuged at 10,000 × g for 1 h at 4 °C, then the supernatants were
178   mixed with pre-cooled acetone/methanol and incubated for 1 h at -20 °C. The mixtures were
179   centrifuged at 15,000 × g for 15 min at 4 °C. The pellets were washed twice with cold acetone.
180   Pellets were dried and solubilised in lysis buffer containing 50 mM Tris-HCl (pH 6.8), 8 M urea,
181   5 mM DTT, 1% SDS, and 10 mM EDTA. Protein concentrations of the samples were estimated
182   using the Bradford method (Bradford, 1976) (Table S1) and the samples were stored at -80 °C for
183   further use. All protein samples were checked via sodium dodecyl sulfate polyacrylamide gel
184   electrophoresis (SDS-PAGE) according to the Schägger protocol (Schägger, 2006). SDS-PAGE
185   gels (Figure S1) were stained with Coomassie Brilliant Blue (CBB) staining solution (Coomassie
186   Blue Fast Staining Solution, Beijing Dingguo Changsheng Biotechnology Co., LTD) (Kang et al.,
187   2002).
188   After determining the protein concentration, we digested the samples with trypsin (Promega,
189   V5113) and then incubated them for 12-16 h at 37 °C. Approximately 100 μg of peptides of the
190   different samples were labelled with iTRAQ based on the protocol of Unwin et al. (Unwin,
191   Griffiths & Whetton, 2010). The peptides of the different samples were labelled with iTRAQ

192   reagents (isobaric tags 113, 114, 115, 116, 117, 118, 119, and 121 for groups YM18-WAS, *ZK001*-
193   WAS, YM18-GAS, *ZK001*-GAS, YM18-YAS, *ZK001*-YAS, YM18-AS, and *ZK001*-AS,
194   respectively) according to the manufacturer's instructions (Applied Biosystems).

195   **HPLC grading of C_{18} columns at high pH and LC-electrospray ionization-MS/MS analysis**
196   The lyophilised peptide mixture was reconstituted with 100 µL of solution A (2% acetonitrile
197   (ACN) and 20 mM ammonium formate, pH 10). Then, the samples were loaded onto a reverse-
198   phase column [C_{18} column, 1.9 µm (particle size), 150 µm (inner diameter) × 120 mm (length),
199   Waters] and eluted using a step linear elution program (Table S2). The samples were collected
200   every 1.5 min and centrifuged at 14,000 × g for 5-90 min. The 60 collected fractions were dried
201   and re-dissolved with 5 µL 0.5% formic acid (FA). The collected fractions were finally combined
202   into 10 pools and centrifuged at 14,000 × g for 10 min.

203   The reconstituted peptides were analysed with a Q-Exactive HF mass spectrometer (Thermo
204   Fisher Scientific) coupled with a nano high-performance liquid chromatography system (1260
205   Infinity II, Agilent) (Scheltema et al., 2014). The peptides were loaded onto a C_{18} reversed-phase
206   column [C_{18} column, 3 µm (particle size), 100 µm (inner diameter) × 200 mm (length), Thermo
207   Scientific] using mobile phases A (0.1% FA/H_2O) and B (0.08% FA, 80% ACN) (Table S3). The
208   HPLC effluent was directly electrosprayed into the mass spectrometer and analysed based on pre-
209   set parameters (Figure S2).

210   **Data analysis**
211   The raw mass data were processed for peptide identification using Proteome Discoverer 1.4 (ver.
212   1.4.0.288, Thermo Fisher Scientific) with specific parameters (Table S4) for searching the UniProt
213   Triticum database. A false discovery rate (FDR) of ≤ 0.01 was estimated for protein identification
214   using a target-decoy search strategy (Elias & Gygi, 2007). The mass spectrometry proteomics data
215   have   been   deposited   in   the   ProteomeXchange   Consortium
216   (http://proteomecentral.proteomexchange.org) via the PRIDE partner repository (Vizcaino et al.,
217   2016) with the dataset identifier < PXD010188 >. Increasing and decreasing abundant proteins
218   were determined based on 1.5-fold-changes and peptides spectral matches (PSMs) ≥ 2 (Sharma et
219   al., 2017) between *ZK001*-WAS and YM18-WAS (Group 1), *ZK001*-GAS and YM18-GAS
220   (Group 2), *ZK001*-YAS and YM18-YAS (Group 3), *ZK001*-AS and YM18-AS (Group 4), YM18-
221   WAS and YM18-GAS (Group 5), YM18-WAS and YM18-YAS (Group 6), YM18-WAS and
222   YM18-AS (Group 7), *ZK001*-WAS and *ZK001*-GAS (Group 8), *ZK001*-WAS and *ZK001*-YAS
223   (Group 9), and *ZK001*-WAS and *ZK001*-AS (Group 10).

224   Protein annotation was conducted by a BLAST search against NCBI and UniProt databases.
225   Protein   function   was   classified   based   on   the   following   databases: Gene   Ontology
226   (http://www.geneontology.org/, GO), and Kyoto Encyclopedia of Genes and Genomes
227   (http://www.genome.jp/kegg/, KEGG). For analysis of differentially abundant proteins (DAPs),
228   significant GO enrichment and KEGG enrichment were defined as a corrected FDR with a *P*–
229   value less than 0.01 (Benjamini & Hochberg, 1995). Proteins containing at least two peptide
230   spectral matches (PSMs) per protein and fold change ratios ≥ 1.5 or ≤ 0.67 were considered more
231   abundant or less abundant proteins, respectively. In order to validate the DAPs profile, we searched

232   the EnsemblPlants database (http://plants.ensembl.org/index.html) for corresponding DNA
233   sequences. A total of 10 DAPs involved in carbohydrate metabolism and calcium ion binding and
234   transport were selected for qRT-PCR validation.

Quantitative real-time PCR validation

236   Total RNA was isolated using a Plant RNA kit (Omega, R6827) according to the manufacturer's
237   instructions. The quality of each RNA sample was checked on 1% agarose gels. Measurement of
238   the concentration of RNA samples was performed using a NanoDrop 2000 spectrophotometer
239   bioanalyzer (Thermo Fisher Scientific). cDNAs were synthesised using TransScript One-Step
240   gDNA Removal and cDNA Synthesis SuperMix (Transgen Biotech) according to the
241   manufacturer's protocol. qRT-PCR was used to measure the transcript levels of the proteins of
242   interest. Each experiment was performed in three technical replicates with three biological
243   replicates. Target gene-specific primers (Table S5) were designed using the online software Primer
244   3 version 0.4.0 (http://bioinfo.ut.ee/primer3-0.4.0/primer3/) (Untergasser et al., 2012).
245   Quantitative reverse transcription polymerase chain reaction (qRT-PCR) was performed according
246   to the manufacturer's instructions for the FastStart Essential DNA Green Master (Roche), run on
247   the Roche LightCycler® 96 Instrument. The *glyceraldehyde-3-phosphate dehydrogenase* gene
248   from *T. aestivum* (*TaGAPDH*, GI: 7579063) served as an internal control and the relative
249   expression of target genes was calculated using the $2^{-\Delta\Delta CT}$ method (Livak & Schmittgen, 2001).

Statistical data analysis

251   The experimental data values represented the average of the measurements conducted from three
252   independent assays and were expressed as the mean ± standard error of the mean (SEM). The data
253   were further analysed using ANOVA followed by Duncan's test (SPSS 18.0, IBM, Somers, NY,
254   USA). The level of significance was set at $P \leq 0.05$.

Results

Comparative resistance to *Fusarium* head blight

257   The results of FHB resistance testing showed that the infection rate in Sumai 3 (SM3) and *ZK001*
258   were 7.03% and 9.39% in 2013-2014 and 8.61% and 17.60% in 2014-2015, respectively (Table
259   1). Compared to SM3 and *ZK001*, YM18 and Aikang (AK58) were highly susceptible: the FHB
260   infection rate was 35.16% and 38.12% in 2014-2015, respectively. However, the diseased spikelet
261   rates for YM18 and AK58 were 15.20% and 20.41% in 2013-2014, respectively, which was half
262   the rate in 2014-2015 (Table 1). This indicates that the FHB infection rate is greatly influenced by
263   environmental factors. These results suggest that cleistogamous cultivars have a lower FHB
264   infection rate than chasmogamous cultivars.

Comparison of flowering in YM18 and *ZK001*

266   In accordance with previous reports, the exserted anthers increased the incidence of FHB (Sage &
267   De Isturiz, 1974; PARRY, JENKINSON & McLEOD, 1995). Furthermore, the anthers of
268   cleistogamy wheat were detained in glums during the flowering stage. Although the individual
269   lines of YM18 and *ZK001* were grown under the same growth and environmental conditions, the
270   morphological differences were obvious. In YM18, the anthers extruded from the palea and lemma
271   at the AS, whereas no anthers were observed in *ZK001* at all flower development stages (Figure

272   1A). The morphology of the lodicules of YM18 and *ZK001* was also obviously different. In order
273   to investigate their morphology, we harvested the lodicules of YM18 and *ZK001* at the GAS and
274   cultured them for 90 minutes on MS medium. The width of the YM18 lodicules (Figure 1B) was
275   greater than that of the *ZK001* lodicules (Figure 1C and 1D).

276   **Physiological characteristics of lodicules in YM18 and *ZK001***
277   To reveal the cause of the lodicules difference between YM18 and *ZK001*, we measured the starch
278   and total soluble sugar contents in the lodicules of YM18 and *ZK001* at the four flower
279   development stages. Lodicule starch (Figure 2A, Table S6) and total soluble sugar (Figure 2B,
280   Table S6) contents showed an overall increase from the WAS to the AS for YM18 and *ZK001*. No
281   significant differences in the starch and soluble sugar contents in the lodicule were observed
282   between YM18 and *ZK001* during the WAS or GAS. Additionally, the starch and total soluble
283   sugar contents in *ZK001* during the YAS significantly decreased 2.40 and 1.75-fold, respectively
284   (both $P<0.05$), compared with those in YM18, detected in one pair of lodicules (Figure 2, Table
285   S6). In contrast, the starch and total soluble sugar contents in *ZK001* during the AS remarkably
286   increased 3.57 and 1.52-fold, respectively (both $P<0.05$), compared with those in YM18, detected
287   in one pair of lodicules (Figure 2, Table S6).

288   **Overview of quantitative proteome analysis**
289   In order to study the protein expression patterns in YM18 and *ZK001*, we examined and
290   quantitatively catalogued the proteomes of YM18 and *ZK001* in the four flower development
291   stages using iTRAQ technology. In this study, 19,422 peptides were matched to 4,497 proteins in
292   the samples (Table S7); in addition, 11,603 unique peptides were found, and 2,172 proteins were
293   identified with more than two unique peptide sequences excluding post-translational
294   modifications. As shown in Figure 3A, more than 99% of the peptides covered proteins within the
295   36 peptides, and protein quantity decreased as the number of matching peptides increased. In terms
296   of protein mass distribution, good coverage (an average of 10%–18% of total proteins in each
297   protein-mass group) was obtained for proteins > 10 kDa and < 60 kDa (Figure 3B). The length of
298   the identified peptides was between 10 and 13 amino acids at the peak and approximately 93% of
299   the peptide length was within 24 amino acids (Figure 3C). Over 77% of the proteins had > 5%
300   sequence coverage. Additionally, sequence coverage distribution was high in most of the identified
301   proteins: More than 58% had over > 10% coverage and more than 37% had over 20% coverage
302   (Figure 3D). These results indicate that the identified peptides were sufficient for protein
303   identification.

304   **Cluster analysis of protein expression at four developmental stages**
305   In order to identify more differentially abundant proteins (DAPs), we compared DAPs in YM18
306   and *ZK001* in the flowering development process, *ZK001*-WAS vs YM18-WAS (Group 1),
307   *ZK001*-GAS vs YM18-GAS (Group 2), *ZK001*-YAS vs YM18-YAS (Group 3), *ZK001*-AS vs
308   YM18-AS (Group 4), YM18-WAS vs YM18-GAS (Group 5), YM18-WAS vs YM18-YAS
309   (Group 6), YM18-WAS vs YM18-AS (Group 7), *ZK001*-WAS vs *ZK001*-GAS (Group 8), *ZK001*-
310   WAS vs *ZK001*-YAS (Group 9), and *ZK001*-WAS vs *ZK001*-AS (Group 10). Increasing
311   abundance and decreasing abundance proteins were determined based on fold-changes (FC) of >

312   1.5 or < 0.667 for expression difference comparison. For further screening, approximately 16, 47,
313   2, 0, 11, 124, 105, 15, 298 and 188 DAPs were identified with a corrected P–value for GO KEGG
314   enrichment less than 0.01 in groups 1 to 10 (Table 2). A Venn diagram of the DAPs and their
315   overlap in Group 1 and Group 2 showed that two common DAPs were increased-abundance and
316   1 common DAP was decreased-abundance (Figure S3). Group 3 and Group 4 showed no overlap
317   with Group 1 or Group 2 (Figure S3). Venn diagrams indicated that 6, 10, 32, 206, 57, and 140
318   DAPs were specific DAPs of Groups 5, 8, 6, 9, 7, and 10, respectively (Figure S3).

319   **Functional classification and subcellular localization of proteins**
320   GO analysis showed that all of the identified proteins in YM18 and *ZK001* were involved in 11
321   subgroups of MF, 19 subgroups of BP, and 14 subgroups of CC (Figure S4). Significant GO
322   enrichment was employed to analyse the DAPs with a corrected FDR P–value less than 0.01 and
323   an FC ratio of more than 1.5. Based on GO annotations and enrichments, the DAPs of Group 1
324   were enriched in molecular function terms for lipid binding (100%) (Figure 4A) as well as
325   biological process terms for lipid transport (14.06%), lipid localization (14.06%), macromolecule
326   localization (20.31%), organic substance transport (20.31%), single-organism transport (15.63%),
327   and single-organism localization (15.63%) (Figure 4B). GO classification of Group 2 revealed that
328   the DAPs were enriched in the biological process, cellular component, and molecular function
329   (Figure 4C). No protein was enriched in Group 3 or Group 4. The DAPs of Groups 5 to 10 were
330   also classified into biological process (Figure S5A), cellular component (Figure S5B) and
331   molecular function (Figure S5C). DAPs involved in carbohydrate metabolism and transport,
332   calcium ion binding and protein transport, and fatty acid biosynthesis were further used in cluster
333   analyses.

334   **Accumulation patterns of DAPs and verification of DAPs of interest**
335   Based on the above analyses, 11 genes which corresponded to DAPs of interest were chosen for
336   qRT-PCR analyses using gene-specific primers (Table S5) to explore the expression profile at the
337   transcription level.
338   The lodicule morphology showed significant differences between YM18 and *ZK001* (Figure
339   1). We performed qRT-PCR using the RNA of YM18 and *ZK001* lodicules to study the transcript
340   profiles of the 11 genes corresponding to the selected DAPs (Figure 5). The results of qRT-PCR
341   indicated that the expression level of the gene *A0A1D6CCI3* (encoding the bidirectional sugar
342   transporter SWEET) was expressed in the lodicules at the WAS and GAS of both YM18 and
343   *ZK001*, with almost no expression at the YAS and AS (Figure 3, Table S7); (Figure 5A).
344   Additionally, the expression level of the gene *A0A1D5WGA3* (encoding a nutrient reservoir-
345   related protein) was extremely down-regulated from the WAS to the GAS in both YM18 and
346   *ZK001* (Figure 5B). Though the relative expression level in *ZK001* was significantly higher than
347   that in YM18 in the GAS ($P<0.001$), the relative expression levels were all less than 0.1 in the
348   GAS, YAS or AS in YM18 or *ZK001* (Figure 5B). Compared with the relative expression levels
349   of the gene encoding beta-amylase A0A1D5RR02 in YM18, the gene in *ZK001* was down-
350   regulated during the WAS ($P<0.001$), GAS ($P<0.05$), YAS ($P<0.05$), and AS ($P<0.05$) (Figure
351   5C). The relative expression levels of *A0A1D5RR02* were all down-regulated from the WAS to

352   the YAS in YM18 and *ZK001*, but there was no significant difference from the YAS to the AS in
353   YM18 or *ZK001* (both *P*>0.05) (Figure 5C). Additionally, compared with its expression in the
354   lodicules of YM18, P93594 (beta-amylase)-encoding mRNA was all up-regulated (*P*<0.001) in
355   the lodicules of *ZK001*, except that in the YAS (Figure 5D). Interestingly, the mRNA level of
356   sucrose synthase W5B5R3 in *ZK001* indicated up-regulation compared with the levels in YM18
357   at the GAS, YAS, and AS (*P*<0.001), and down-regulation at the WAS (*P*<0.05) (Figure 5E). The
358   mRNA levels of *A0A1D5SYC3* (a gene encoding cellular glucose homeostasis-related proteins)
359   and *A0A1D5VEI9* (a gene encoding cellular glucose homeostasis-related proteins) showed almost
360   the same expression profile as *W5B5R3*, except for that of *A0A1D5SYC3* in the WAS and that of
361   *A0A1D5VEI9* in the AS (Figures 5E, 5F, and 5G). The relative expression level of *A0A1D5RVB4*
362   (a gene encoding cellular glucose homeostasis-related proteins) and *W5B5R3* were similar (Figure
363   5E and 5H). Compared with expression levels in YM18, the gene expression of beta-glucosidase
364   activity-related protein A0A077S2F2 in *ZK001* was down-regulated (*P*<0.05) during the WAS
365   and GAS and up-regulated (*P*<0.001) in the AS (Figure 5I).
366   Calcium ions play a key role in the development of plants. Therefore, the relative expression
367   of the genes encoding calcium ion binding-related protein A0A1D5TN57 and annexin
368   A0A1D5RRV7 were also evaluated to determine the profile during flower development.
369   Compared with levels in YM18, the relative gene expression levels of A0A1D5TN57 in *ZK001*
370   were up-regulated during the WAS and YAS(Figure 5K), and those of A0A1D5RRV7 were up-
371   regulated during the WAS, YAS and AS (Figure 5J). However, the expression levels of
372   *A0A1D5RRV7* and *A0A1D5TN57* were all down-regulated (*P*<0.05) from the WAS to the GAS in
373   *ZK001* (Figure 5J and 5K).

Discussion

Cleistogamy provides structural barriers for diseases of *Fusarium* head blight

376   From the physiological point of view, the flowering stage is regarded as the most susceptible period
377   for primary infection of wheat spikes by FHB because of the opening of wheat florets and the
378   extension of anthers (Pugh, Johann & Dickson, 1933; Schroeder & Christensen, 1963; Gilsinger
379   et al., 2005; Schuster & Ellner, 2008). Barley is a plant that self-fertilizes with permanently closed
380   flowers, but chasmogamous barley varieties are easily infected with *Fusarium* (Yoshida, Kawada
381   & Tohnooka, 2005; Culley & Klooster, 2007). Table 1 shows that the diseased spikelet rate in
382   2014-2015 was more severe than that in 2013-2014 except in SM3, possibly because of the
383   resistance gene *Fhb1* (Rawat et al., 2016). Compared with YM18, which is a wild-type
384   chasmogamous cultivar, the diseased spikelet rate for *ZK001*, a mutant cleistogamous cultivar,
385   decreased by 38.22% and 50.00% in 2013-2014 and 2014-2015, respectively (Table 1). This
386   indicates that although the diseased spikelet rate is greatly influenced by environmental factors,
387   cleistogamous cultivars that flower partially or completely may have a lower risk of FHB infection
388   than chasmogamous cultivars (Kubo et al., 2010; Wang et al., 2013). Therefore, we further verified
389   the hypothesis that cleistogamous wheat cultivars might have lower *Fusarium* susceptibility. A
390   practical strategy for controlling FHB would be to introduce the cleistogamous character into other
391   varieties that are suitable for production and promotion but sensitive to FHB through hybridization.

Lodicules play an important role in glume opening/closing in wheat

The molecular mechanism for cleistogamy has been intensively studied in rice (Maeng et al., 2006; Yoshida et al., 2007; Ohmori et al., 2012; Ni et al., 2014; Lombardo et al., 2017) and barley (Turuspekov et al., 2004; Hori et al., 2005; Nair et al., 2010; Wang et al., 2013, 2015; Zhang et al., 2016). However, the molecular mechanism for cleistogamy in wheat remains unclear, though it is known that the lodicule is a key factor in glume opening/closing in the monocotyledon. The abnormal lodicules may lack the ability to push the lemma and palea apart during the flowering stage in the cleistogamous mutant *ZK001* (Figure 1). This phenomenon is similar to that occurring in barley (Nair et al., 2010).

Carbohydrates and calcium are the main factors regulating lodicule osmotic pressure

Sucrose is the primary form of sugar transported for photosynthetic carbon assimilation (Chen et al., 2012). The *A0A1D6CCI3* gene was expressed in the lodicules of both YM18 and *ZK001* (Figure 5A, Table S8). This indicates that carbohydrates can be transferred normally to the lodicules of both YM18 and *ZK001*. Nevertheless, the starch (Figure 2A, Table S6) and soluble sugar (Figure 2B, Table S6) contents of the YM18 lodicules increased dramatically from the GAS to the YAS. Liu et al. (Liu et al., 2017) suggested that retarded lodicule expansion in *ZS97A* was caused by reduced water accumulation because of diminished accumulation of osmotic regulation substances. In contrast, the lower soluble sugar content in the lodicules of *ZK001* prevented the accumulation of water during the YAS (Figure 2B, Table S6). The lodicule size of YM18 was larger than that of *ZK001* because the starch and soluble sugar contents in the lodicules of *ZK001* decreased from the GAS to the YAS, leading to little water transfer to the lodicules. The lodicules of wheat swell extensively and subsequently contract after rapid autolysis of the tissues (Craig & O'Brien, 1975). Accordingly, the starch and soluble sugar contents in the lodicule of YM18 were lower than those in *ZK001* at the AS (Figure 2A and 2B, Table S6).

Cytosolic calcium is an important secondary messenger in plants and plays important roles in the response to both environmental and internal signals (Poovaiah & Reddy, 1993; Liao, Zheng & Guo, 2017). Plant annexins are calcium-dependent phospholipid binding proteins with many biological functions; for instance, they participate in calcium ion channel formation, membrane dynamics, plant growth and the stress response (Mortimer et al., 2008; Laohavisit & Davies, 2011). In this study, the relative gene expression levels of annexin (A0A1D5RRV7) and the calcium ion binding-related protein (A0A1D5TN57) in the lodicules of *ZK001* were up-regulated during the WAS compared to those of in the lodicules of YM18 (Figures 5J and 5K). Therefore, we infer that the WAS is a critical period for the lodicules.

An overview of the pathways for proteome metabolic changes in lodicules

Many substances regulate the osmotic pressure of lodicules, such as soluble sugar (Zee & O'Brien, 1971; Wang, Gu & Gao, 1991; Yan et al., 2017), starch (Pissarek, 1971), calcium (Qin, Yang & Zhao, 2005; Chen et al., 2016) and potassium (Heslop-Harrison & Heslop-Harrison, 1996; Chen et al., 2016; Liu et al., 2017). Our findings, together with those of previous studies, provide an overview of the metabolic pathways involving the carbohydrates that regulate the osmotic pressure of the lodicules. As shown in Figure 6, sucrose is transferred into the lodicules from the extra-

432 cellular environment through a bidirectional sugar transporter (A0A1D6CCI3), and is converted
433 into D-fructose-6P by hexokinase (A0A1D5SYC3, A0A1D5RVB4 and A0A1D5VEI9) after being
434 broken down into D-fructose. D-fructose-6P converted to α-D-glucose-1P, which can be converted
435 to D-glucose by β-glucosidase (A0A077S2F2) and synthesised into amylose. The starch formed
436 from amylose can be broken down into D-glucose under the action of β-amylase (A0A1D5RR02
437 and P93594). UDP-glucose formed from amino sugar and nucleotide sugar can also be converted
438 into D-glucose under the action of β-glucosidase (A0A077S2F2). The accumulation of D-glucose
439 leads to a change in osmotic pressure in the lodicules. Additionally, α-D-glucose-1P can enter the
440 pentose phosphate pathway and the fatty acid biosynthesis pathway through the formation of α-D-
441 glucose-6P and β-D-glucose-6P. Soluble sugar can also enter and exit cells through the
442 bidirectional sugar transporter. Furthermore, annexin (A0A1D5RRV7) can trigger calcium ion
443 influx, increasing the osmotic pressure. Once the osmotic pressure changes, water accumulates in
444 / is excreted from the cells of the lodicules and induces the expansion / shrinkage of the lodicules.
445

Conclusions

447 The wheat mutant, *ZK001*, with its atrophied, thin and ineffective lodicules has lost the ability to
448 push the lemma and palea apart in the flower development process. Compared with YM18, *ZK001*
449 showed a lower rate of *Fusarium* infection, presumably because of the cleistogamous phenotype.
450 Furthemore, we speculate that the thin lodicule of *ZK001* results from its lower soluble sugar,
451 calcium ion, and potassium ion contents, which are regulated by carbohydrate metabolic, protein
452 transport, and calcium ion binding-related proteins. Though little is known about the mechanism
453 of cleistogamy in wheat, we propose an overview of the metabolic pathway involving the
454 carbohydrate that regulates the osmotic pressure of the lodicules. This study provides foundations
455 for researchers to explore the mechanism of cleistogamy. Furthermore, it shows that it should be
456 possible to generate cleistogamous wheat via conventional crossing, which would improve the
457 FHB resistance of wheat and control the pollen-mediated gene flow of genetically modified wheat.
458

Acknowledgements

460 We thank Prof. Xiue Wang, College of Agriculture, Nanjing Agricultural University, for providing
461 FHB spore F0601. We thank Mr. Shiliang Li and Ms. Shengqun Zheng for field management. We
462 also thank Mrs. Youwei Wu (graphic designer) for instruction in drawing the Figure 6.

463

References

465 Benjamini Y, Hochberg Y. 1995. Controlling the False Discovery Rate - a Practical and
466   Powerful Approach to Multiple Testing. *Journal of the Royal Statistical Society Series B-*
467   *Methodological* 57:289–300.
468 Bradford MM. 1976. Rapid and sensitive method for quantitation of microgram quantities of
469   protein utilizing principle of protein-dye binding. *Analytical Biochemistry* 72:248–254.
470   DOI: 10.1006/abio.1976.9999.
471 Canovas FM, Dumas-Gaudot E, Recorbet G, Jorrin J, Mock HP, Rossignol M. 2004. Plant
472   proteome analysis. *Proteomics* 4:285–298. DOI: 10.1002/pmic.200300602.

473 Chen Y, Ma J, Miller AJ, Luo B, Wang M, Zhu Z, Ouwerkerk PB. 2016. *OsCHX14* is Involved
474   in the K⁺ Homeostasis in Rice (*Oryza sativa*) Flowers. *Plant Cell Physiol* 57:1530–1543.
475   DOI: 10.1093/pcp/pcw088.
476 Chen LQ, Qu XQ, Hou BH, Sosso D, Osorio S, Fernie AR, Frommer WB. 2012. Sucrose Efflux
477   Mediated by SWEET Proteins as a Key Step for Phloem Transport. *Science* 335:207–211.
478   DOI: 10.1126/science.1213351.
479 Craig S, O'Brien TP. 1975. The Lodicules of Wheat: Pre- and Post-Anthesis. *Australian Journal*
480   *of Botany* 23:451–458. DOI: 10.1071/BT9750451.
481 Culley TM, Klooster MR. 2007. The cleistogamous breeding system: A review of its frequency,
482   evolution, and ecology in angiosperms. *Botanical Review* 73:1. DOI: 10.1663/0006-
483   8101(2007)73[1:TCBSAR]2.0.CO;2.
484 Diallo AO, Agharbaoui Z, Badawi MA, Ali-Benali MA, Moheb A, Houde M, Sarhan F. 2014.
485   Transcriptome analysis of an *mvp* mutant reveals important changes in global gene
486   expression and a role for methyl jasmonate in vernalization and flowering in wheat. *J Exp*
487   *Bot* 65:2271–2286. DOI: 10.1093/jxb/eru102.
488 Elias JE, Gygi SP. 2007. Target-decoy search strategy for increased confidence in large-scale
489   protein identifications by mass spectrometry. *Nat Methods* 4:207–214. DOI:
490   10.1038/nmeth1019.
491 FAO. 2015. *FAO statistical pocketbook, World food and agriculture 2015, Rome, Food and*
492   *Agricultural Organization of the United Nations*.
493 Feng YL, Wang KT, Ma C, Zhao YY, Yin J. 2015. Virus-induced gene silencing-based
494   functional verification of six genes associated with vernalization in wheat. *Biochem Biophys*
495   *Res Commun* 458:928–933. DOI: 10.1016/j.bbrc.2015.02.064.
496 Gilsinger J, Kong L, Shen X, Ohm H. 2005. DNA markers associated with low *Fusarium* head
497   blight incidence and narrow flower opening in wheat. *Theoretical and Applied Genetics*
498   110:1218–1225. DOI: 10.1007/s00122-005-1953-4.
499 Guo Z, Schnurbusch T. 2015. Variation of floret fertility in hexaploid wheat revealed by tiller
500   removal. *J Exp Bot* 66:5945–5958. DOI: 10.1093/jxb/erv303.
501 Heslop-Harrison Y, Heslop-Harrison JS. 1996. Lodicule Function and Filament Extension in the
502   Grasses: Potassium Ion Movement and Tissue Specialization. *Annals of Botany* 77:573–
503   582. DOI: 10.1006/anbo.1996.0072.
504 Hollingsworth CR, Motteberg CD, Wiersma J V, Atkinson LM. 2008. Agronomic and Economic
505   Responses of Spring Wheat to Management of *Fusarium* Head Blight. *Plant Disease*
506   92:1339–1348. DOI: 10.1094/PD1S-92-9-l339.
507 Hori K, Kobayashi T, Sato K, Takeda K. 2005. QTL analysis of *Fusarium* head blight resistance
508   using a high-density linkage map in barley. *Theor Appl Genet* 111:1661–1672. DOI:
509   10.1007/s00122-005-0102-4.
510 Kang DH, Gho YS, Suh MK, Kang CH. 2002. Highly sensitive and fast protein detection with
511   coomassie brilliant blue in sodium dodecyl sulfate-polyacrylamide gel electrophoresis.
512   *Bulletin of the Korean Chemical Society* 23:1511–1512. DOI:
513   10.5012/bkcs.2002.23.11.1511.
514 Kirby EJM, Appleyard M. 1987. *Cereal Development Guide*. 2nd ed Stoneleigh, UK: NAC
515   Cereal Unit, 85pp.
516 Kubo K, Kawada N, Fujita M, Hatta K, Oda S, Nakajima T. 2010. Effect of cleistogamy on
517   *Fusarium* head blight resistance in wheat. *Breed Sci* 60:405–411. DOI:
518   10.1270/jsbbs.60.405.

519   Kumar RR, Goswami S, Sharma SK, Kala YK, Rai GK, Mishra DC, Grover M, Singh GP,
520   Pathak H, Rai A, Chinnusamy V, Rai RD. 2015. Harnessing Next Generation Sequencing in
521   Climate Change: RNA-Seq Analysis of Heat Stress-Responsive Genes in Wheat (*Triticum
522   aestivum* L.). *OMICS* 19:632–647. DOI: 10.1089/omi.2015.0097.
523   Laohavisit A, Davies JM. 2011. Annexins. *New Phytologist* 189:40–53. DOI: 10.1111/j.1469-
524   8137.2010.03533.x.
525   Li QY, Qin Z, Jiang YM, Shen CC, Duan ZB, Niu JS. 2014. Screening wheat genotypes for
526   resistance to black point and the effects of diseased kernels on seed germination. *Journal of
527   Plant Diseases & Protection* 121:79–88. DOI: 10.1007/BF03356495.
528   Liao C, Zheng Y, Guo Y. 2017. *MYB30* transcription factor regulates oxidative and heat stress
529   responses through ANNEXIN‐mediated cytosolic calcium signaling in *Arabidopsis*. *New
530   Phytologist* 216:163. DOI: 10.1111/nph.14679.
531   Liu L, Zou ZS, Qian K, Xia C, He Y, Zeng HL, Zhou X, Riemann M, Yin CX. 2017. Jasmonic
532   acid deficiency leads to scattered floret opening time in cytoplasmic male sterile rice
533   Zhenshan 97A. *Journal of Experimental Botany* 68:4613–4625. DOI: 10.1093/jxb/erx251.
534   Livak KJ, Schmittgen TD. 2001. Analysis of relative gene expression data using real-time
535   quantitative PCR and the $2^{-\Delta\Delta CT}$ Method. *Methods* 25:402–408. DOI:
536   10.1006/meth.2001.1262.
537   Lombardo F, Kuroki M, Yao SG, Shimizu H, Ikegaya T, Kimizu M, Ohmori S, Akiyama T,
538   Hayashi T, Yamaguchi T, Koike S, Yatou O, Yoshida H. 2017. The *superwoman1-
539   cleistogamy 2* mutant is a novel resource for gene containment in rice. *Plant Biotechnology
540   Journal* 15:97–106. DOI: 10.1111/pbi.12594.
541   Ma J, Li R, Wang H, Li D, Wang X, Zhang Y, Zhen W, Duan H, Yan G, Li Y. 2017.
542   Transcriptomics Analyses Reveal Wheat Responses to Drought Stress during Reproductive
543   Stages under Field Conditions. *Front Plant Sci* 8:592. DOI: 10.3389/fpls.2017.00592.
544   Maeng JY, Won YJ, Piao R, Cho YI, Jiang W, Chin JH, Koh HJ. 2006. Molecular mapping of a
545   gene "*ld(t)*" controlling cleistogamy in rice. *Theoretical and Applied Genetics* 112:1429–
546   1433. DOI: 10.1007/s00122-006-0244-z.
547   Mortimer JC, Laohavisit A, Macpherson N, Webb A, Brownlee C, Battey NH, Davies JM. 2008.
548   Annexins: multifunctional components of growth and adaptation. *Journal of Experimental
549   Botany* 59:533. DOI: 10.1093/jxb/erm344.
550   Muqaddasi QH, Brassac J, Borner A, Pillen K, Roder MS. 2017. Genetic Architecture of Anther
551   Extrusion in Spring and Winter Wheat. *Front. Plant Sci* 8:754. DOI:
552   10.3389/fpls.2017.00754.
553   Nair SK, Wang N, Turuspekov Y, Pourkheirandish M, Sinsuwongwat S, Chen G, Sameri M,
554   Tagiri A, Honda I, Watanabe Y, Kanamori H, Wicker T, Stein N, Nagamura Y, Matsumoto
555   T, Komatsuda T. 2010. Cleistogamous flowering in barley arises from the suppression of
556   microRNA-guided *HvAP2* mRNA cleavage. *Proceedings of the National Academy of
557   Sciences of the United States of America* 107:490–495. DOI: 10.1073/pnas.0909097107.
558   Ni DH, Li J, Duan YB, Yang YC, Wei PC, Xu RF, Li CR, Liang DD, Li H, Song FS, Ni JL, Li
559   L, Yang JB. 2014. Identification and utilization of cleistogamy gene *cl7(t)* in rice (*Oryza
560   sativa* L.). *J Exp Bot* 65:2107–2117. DOI: 10.1093/jxb/eru074.
561   Ning S, Wang N, Sakuma S, Pourkheirandish M, Wu J, Matsumoto T, Koba T, Komatsuda T.
562   2013. Structure, transcription and post-transcriptional regulation of the bread wheat
563   orthologs of the barley cleistogamy gene *Cly1*. *Theoretical and Applied Genetics* 126:1273–
564   1283. DOI: 10.1007/s00122-013-2052-6.

565 Ohmori S, Tabuchi H, Yatou O, Yoshida H. 2012. Agronomic traits and gene containment
566   capability of cleistogamous rice lines with the *superwoman1-cleistogamy* mutation. *Breed*
567   *Sci* 62:124–132. DOI: 10.1270/jsbbs.62.124.
568 PARRY DW, JENKINSON P, McLEOD L. 1995. *Fusarium* ear blight (scab) in small grain
569   cereals—a review. *Plant Pathology* 44:207–238. DOI: doi:10.1111/j.1365-
570   3059.1995.tb02773.x.
571 Pissarek HP. 1971. Untersuchungen über Bau und Funktion der Gramineen-Lodiculae. *Beitrage*
572   *Zur Biologie Der Pflanzen* 47:313–370.
573 Poovaiah BW, Reddy ASN. 1993. Calcium and Signal-Transduction in Plants. *Critical Reviews*
574   *in Plant Sciences* 12:185–211. DOI: Doi 10.1080/713608046.
575 Pugh GW, Johann H, Dickson JG. 1933. Factors affecting infection of Wheat heads by
576   *Gibberella saubiuetii. J Agric Res* 46:771–797.
577 Qin Y, Yang J, Zhao J. 2005. Calcium changes and the response to methyl jasmonate in rice
578   lodicules during anthesis. *Protoplasma* 225:103–112. DOI: 10.1007/s00709-005-0086-6.
579 Rawat N, Pumphrey MO, Liu S, Zhang X, Tiwari VK, Ando K, Trick HN, Bockus WW,
580   Akhunov E, Anderson JA, Gill BS. 2016. Wheat Fhb1 encodes a chimeric lectin with
581   agglutinin domains and a pore-forming toxin-like domain conferring resistance to *Fusarium*
582   head blight. *Nat Genet* 48:1576–1580. DOI: 10.1038/ng.3706.
583 Sage GCM, De Isturiz MJ. 1974. The inheritance of anther extrusion in two spring wheat
584   varieties. *Theoretical and Applied Genetics* 45:126–133. DOI: 10.1007/bf00291142.
585 Schägger H. 2006. Tricine-SDS-PAGE. *Nature Protocols* 1:16–22. DOI: 10.1038/nprot.2006.4.
586 Scheltema RA, Hauschild JP, Lange O, Hornburg D, Denisov E, Damoc E, Kuehn A, Makarov
587   A, Mann M. 2014. The Q Exactive HF, a Benchtop Mass Spectrometer with a Pre-filter,
588   High-performance Quadrupole and an Ultra-high-field Orbitrap Analyzer. *Molecular &*
589   *Cellular Proteomics* 13:3698–3708. DOI: 10.1074/mcp.M114.043489.
590 Schroeder HW, Christensen JJ. 1963. Factors affecting resistance of Wheat to scab caused by
591   *Gibberella zeae. Phytopathology* 53:831.
592 Schuster R, Ellner FM. 2008. Level of *Fusarium* infection in wheat spikelets related to location
593   and number of inoculated spores. *Mycotoxin Research* 24:80–87. DOI:
594   10.1007/BF02985285.
595 Schweppe RE, Haydon CE, Lewis TS, Resing KA, Ahn NG. 2003. The characterization of
596   protein post-translational modifications by mass spectrometry. *Acc Chem Res* 36:453–461.
597   DOI: 10.1021/ar020143l.
598 Sharma M, Gupta SK, Majumder B, Maurya VK, Deeba F, Alam A, Pandey V. 2017. Salicylic
599   acid mediated growth, physiological and proteomic responses in two wheat varieties under
600   drought stress. *J Proteomics* 163:28–51. DOI: 10.1016/j.jprot.2017.05.011.
601 Turuspekov Y, Mano Y, Honda I, Kawada N, Watanabe Y, Komatsuda T. 2004. Identification
602   and mapping of cleistogamy genes in barley. *Theoretical and Applied Genetics* 109:480–
603   487. DOI: 10.1007/s00122-004-1673-1.
604 Untergasser A, Cutcutache I, Koressaar T, Ye J, Faircloth BC, Remm M, Rozen SG. 2012.
605   Primer3--new capabilities and interfaces. *Nucleic Acids Research* 40:e115. DOI:
606   10.1093/nar/gks596.
607 Unwin RD, Griffiths JR, Whetton AD. 2010. Simultaneous analysis of relative protein
608   expression levels across multiple samples using iTRAQ isobaric tags with 2D nano LC-
609   MS/MS. *Nature Protocols* 5:1574–1582. DOI: 10.1038/nprot.2010.123.

610 Vizcaino JA, Csordas A, del-Toro N, Dianes JA, Griss J, Lavidas I, Mayer G, Perez-Riverol Y,
611   Reisinger F, Ternent T, Xu QW, Wang R, Hermjakob H. 2016. 2016 update of the PRIDE
612   database and its related tools. *Nucleic Acids Research* 44:D447–D456. DOI:
613   10.1093/nar/gkv1145.
614 Walter S, Nicholson P, Doohan FM. 2010. Action and reaction of host and pathogen during
615   *Fusarium* head blight disease. *New Phytol* 185:54–66. DOI: 10.1111/j.1469-
616   8137.2009.03041.x.
617 Wang Z, Gu Y, Gao Y. 1991. Studies on the mechanism of the anthesis of rice III. structure of
618   the lodicule and changes of its contents during flowering. *Acta Agronomica Sinica* 17:96–
619   101.
620 Wang N, Ning S, Pourkheirandish M, Honda I, Komatsuda T. 2013. An alternative mechanism
621   for cleistogamy in barley. *Theoretical and Applied Genetics* 126:2753–2762. DOI:
622   10.1007/s00122-013-2169-7.
623 Wang N, Ning S, Wu J, Tagiri A, Komatsuda T. 2015. An epiallele at *cly1* affects the expression
624   of floret closing (cleistogamy) in barley. *Genetics* 199:95–104. DOI:
625   10.1534/genetics.114.171652.
626 Winfield MO, Lu C, Wilson ID, Coghill JA, Edwards KJ. 2010. Plant responses to cold:
627   Transcriptome analysis of wheat. *Plant Biotechnol J* 8:749–771. DOI: 10.1111/j.1467-
628   7652.2010.00536.x.
629 Won YJ, Koh HJ. 1998. Inheritance of cleistogamy and its interrelationship between other
630   agronomic characters in rice. *Korean Journal of Breeding*.
631 Wu WW, Wang GH, Baek SJ, Shen RF. 2006. Comparative study of three proteomic
632   quantitative methods, DIGE, cICAT, and iTRAQ, using 2D gel- or LC-MALDI TOF/TOF.
633   *Journal of Proteome Research* 5:651–658. DOI: 10.1021/pr050405o.
634 Yan S, Tang Z, Su W, Sun W. 2005. Proteomic analysis of salt stress-responsive proteins in rice
635   root. *Proteomics* 5:235–244. DOI: 10.1002/pmic.200400853.
636 Yan H, Zhang B, Zhang Y, Chen X, Xiong H, Matsui T, Tian X. 2017. High Temperature
637   Induced Glume Closure Resulted in Lower Fertility in Hybrid Rice Seed Production. *Front
638   Plant Sci* 7:1960. DOI: 10.3389/fpls.2016.01960.
639 Yang Z, Guo GY, Zhang MY, Liu CY, Hu Q, Lam H, Cheng H, Xue Y, Li JY, Li N. 2013.
640   Stable Isotope Metabolic Labeling-based Quantitative Phosphoproteomic Analysis of
641   Arabidopsis Mutants Reveals Ethylene-regulated Time-dependent Phosphoproteins and
642   Putative Substrates of Constitutive Triple Response 1 Kinase. *Molecular & Cellular
643   Proteomics* 12:3559–3582. DOI: 10.1074/mcp.M113.031633.
644 Yang Z, Peng Z, Wei S, Liao M, Yu Y, Jang Z. 2015. Pistillody mutant reveals key insights into
645   stamen and pistil development in wheat (*Triticum aestivum* L.). *BMC Genomics* 16:211.
646   DOI: 10.1186/s12864-015-1453-0.
647 Yoshida H, Itoh J, Ohmori S, Miyoshi K, Horigome A, Uchida E, Kimizu M, Matsumura Y,
648   Kusaba M, Satoh H, Nagato Y. 2007. *superwoman1-cleistogamy*, a hopeful allele for gene
649   containment in GM rice. *Plant Biotechnol J* 5:835–846. DOI: 10.1111/j.1467-
650   7652.2007.00291.x.
651 Yoshida M, Kawada N, Tohnooka T. 2005. Effect of row type, flowering type and several other
652   spike characters on resistance to *Fusarium* head blight in barley. *Euphytica* 141:217–227.
653   DOI: 10.1007/s10681-005-7008-8.

654 Yu SQ, Ma ZH, Zhang M, Peng H, Chai CL, Cui YJ. 2019. Occurring characteristics of wheat
655   scab and its integrated controlling techniques in Henan province. *China plant protection*
656   39:53-60. (Chinese)
657 Yumurtaci A, Sipahi H, Al-Abdallat A, Jighly A, Baum M. 2017. Construction of new EST-
658   SSRs for *Fusarium* resistant wheat breeding. *Comput Biol Chem* 68:22–28. DOI:
659   10.1016/j.compbiolchem.2017.02.003.
660 Zadoks JC, Chang TT, Konzak CF. 1974. A decimal code for the growth stages of cereals. *Weed*
661   *Research* 14:415–421.
662 Zange BJ, Kang Z, Buchenauer H. 2005. Effect of Folicur® on infection process of *Fusarium*
663   culmorum in wheat spikes / Wirkung von Folicur® auf den Infektionsprozess von *Fusarium*
664   culmorum in Weizenähren. *Zeitschrift Für Pflanzenkrankheiten Und Pflanzenschutz*
665   112:52–64.
666 Zee S, O'Brien T. 1971. The Vascular Tissue of the Lodicules of Wheat. *Australian Journal of*
667   *Biological Sciences* 24:797–804.
668 Zhang X, Guo B, Lan G, Li H, Lin S, Ma J, Lv C, Xu R. 2016. A Major QTL, Which Is Co-
669   located with *cly1*, and Two Minor QTLs Are Associated with Glume Opening Angle in
670   Barley (*Hordeum vulgare* L.). *Front. Plant Sci* 7:1585. DOI: 10.3389/fpls.2016.01585.
671 Zhang H, Han B, Wang T, Chen S, Li H, Zhang Y, Dai S. 2012. Mechanisms of plant salt
672   response: insights from proteomics. *J Proteome Res* 11:49–67. DOI: 10.1021/pr200861w.
673 Zhao Q, Zhang H, Wang T, Chen S, Dai S. 2013. Proteomics-based investigation of salt-
674   responsive mechanisms in plant roots. *J Proteomics* 82:230–253. DOI:
675   10.1016/j.jprot.2013.01.024.
676
677
678

Figure 1

Characteristics of genotypes in the 2 differential individual lines of YM18 and *ZK001*.

Comparison of the inflorescence details between YM18 and *ZK001* in post-anthesis stage (Bar = 1 cm) (**A**). Lodicules of YM18 (**B**) and *ZK001* (**C**) which were sampled in GAS and cultured on MS media containing graphite were observed after 90 minutes by microscope (Bar = 1 mm). (**D**) Comparison of lodicule width between YM18 (white column) and *ZK001* (gray column). The results presented are the means of four independent experiments expressed as the mean ± standard error of the mean (SEM). The data were further analyzed using an ANOVA at a 95% confidence level following Duncan's test (SPSS 18.0, IBM, Somers, NY, USA). The level of significance was set at $P \leq 0.05$ or $P \leq 0.001$.
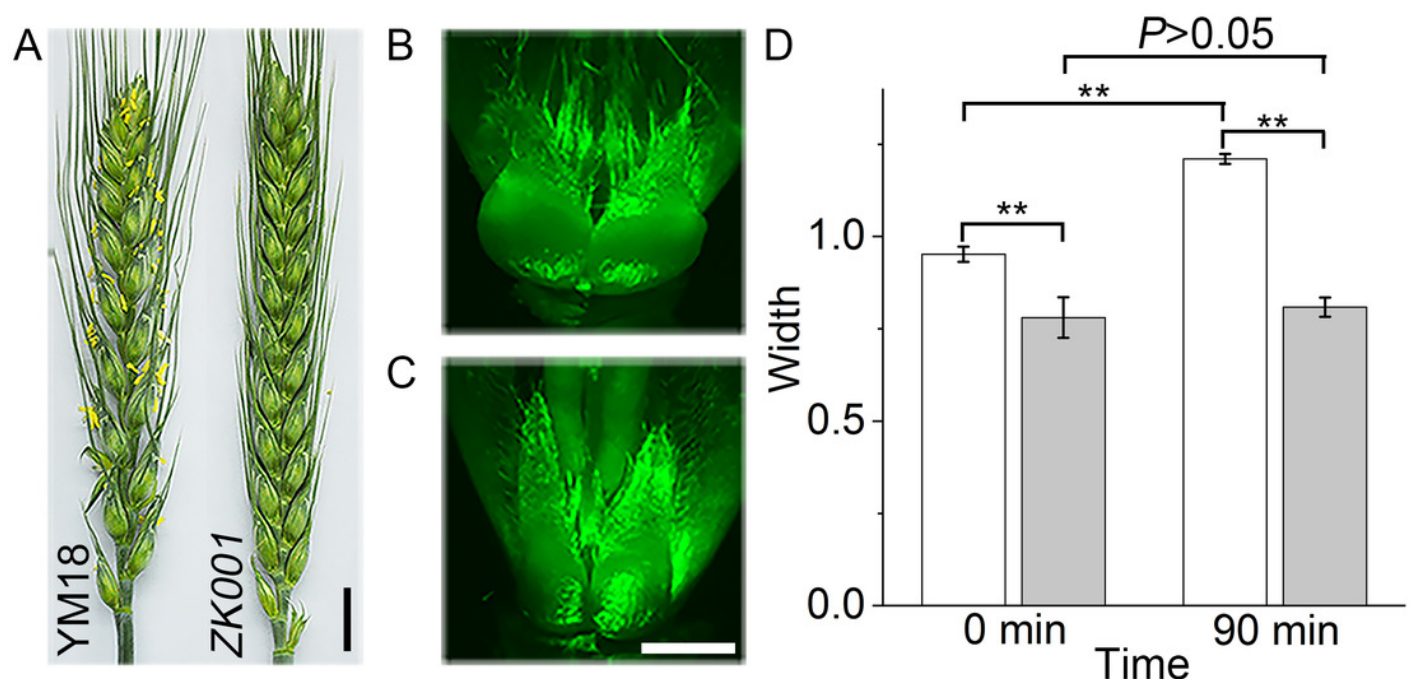
Figure 2

Starch, soluble sugar content in lodicules of YM18 (gray column) and *ZK001* (black column).

A: comparison of starch content change tendency in lodicules between YM18 and *ZK001*. **B:** comparison of soluble sugar content change tendency in lodicules between YM18 and *ZK001*.

PL[1]: pair of lodicules (PL). The results presented are the means of three independent experiments. Error bars, s.d. Columns marked with different lowercase letter indicate difference in means using the one-way ANOVA LSD analysis of PASW Statistics software among four flower development stage of YM18 (gray lowercase) and *ZK001* (black lowercase). The asterisk indicates the difference between YM18 and *ZK001* at WAS, GAS, YAS and AS, respectively. The data were further analyzed using an ANOVA at a 95% confidence level following Duncan's test (SPSS 18.0, IBM, Somers, NY, USA). The level of significance was set at $P \leq 0.05$ or $P \leq 0.001$.
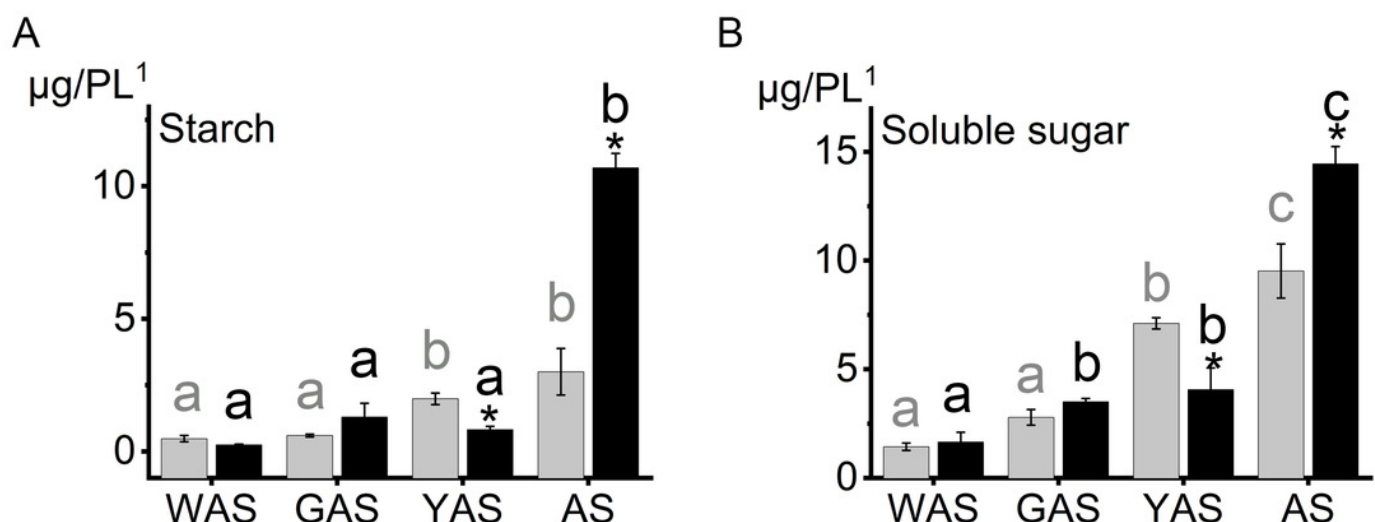
Figure 3

Assessment of iTRAQ analysis for peptides identification and quantitation.

A: The distribution of the identification peptide segments counts corresponding to the identification of proteins number. **B**: Distribution of protein's molecular weight. **C**: Quantification of peptide-length coverage in the identified proteins. **D**: Coverage of protein mass distribution.
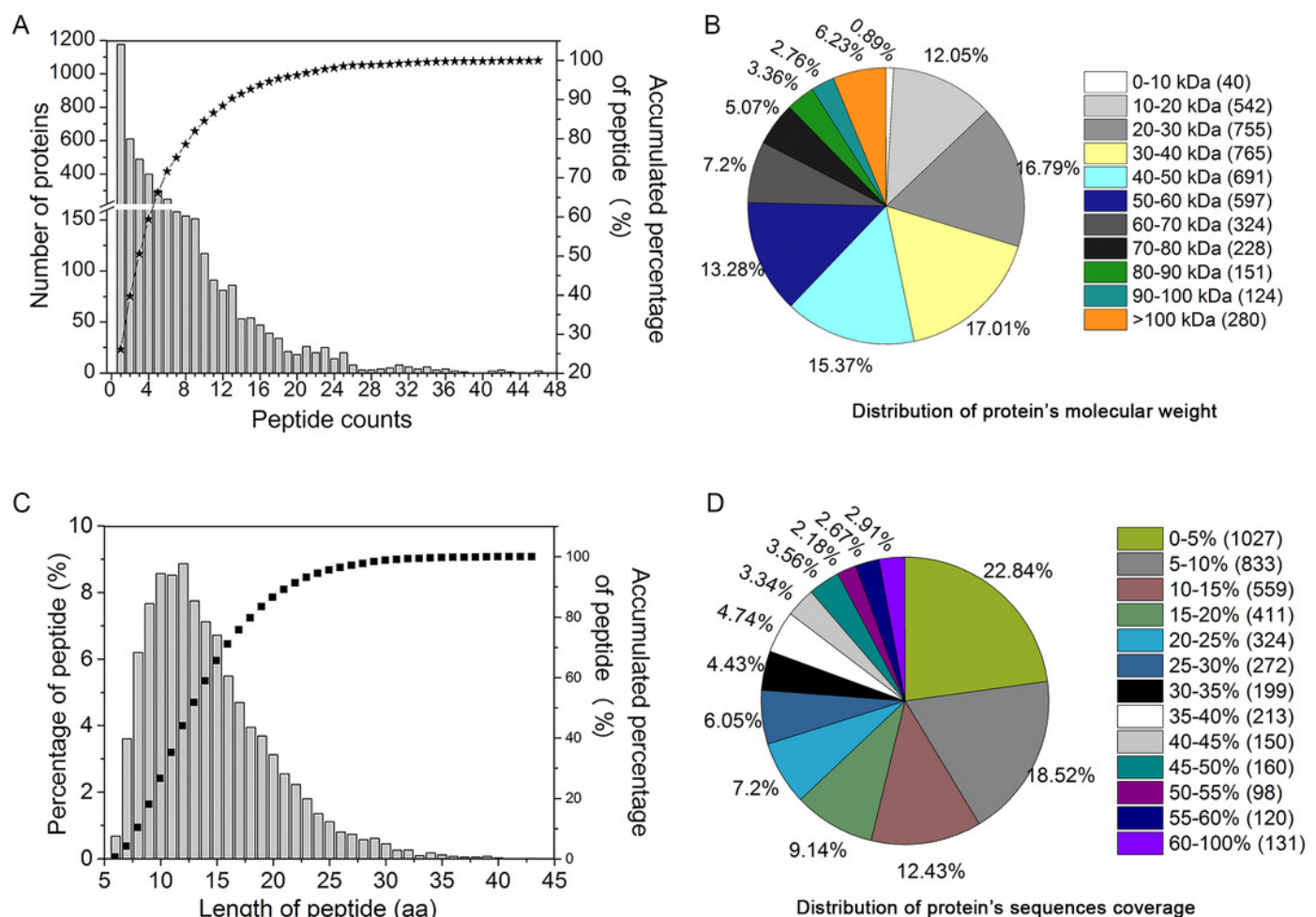
Figure 4

GO classification of DAPs of Group 1 to 4 from four flower development stages in YM18 and *ZK001* based on GO enrichment.

A: molecular function of Group 1; **B**: biological process of Group 1; **C**: biological process, cellular component and molecular function of Group 2. No protein was enriched in Group 3 or Group 4 basing on GO enrichment. (0.667 < FC < 1.5, corrected *P*–value < 0.01, PSMs ≥ 2).
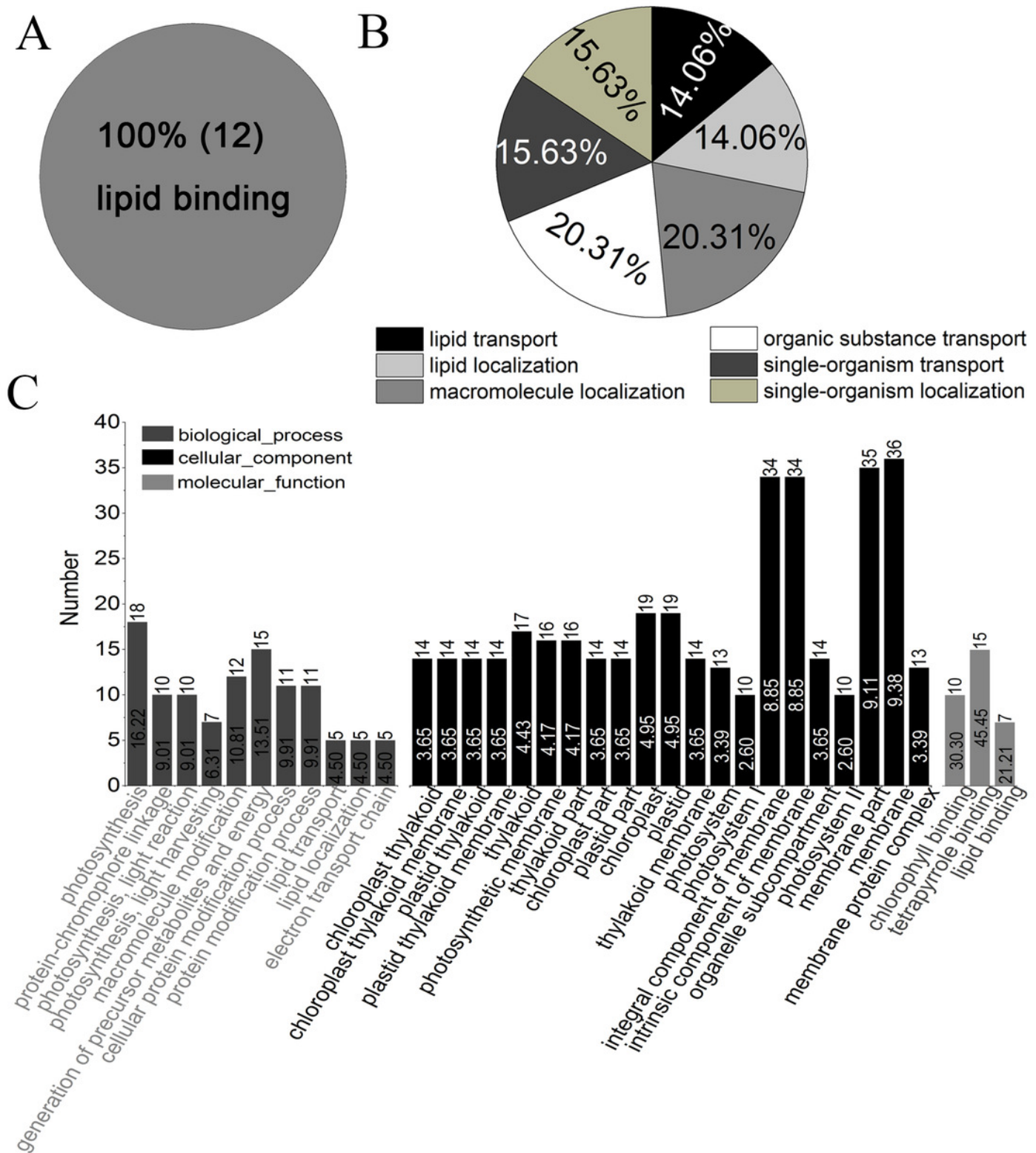
Figure 5

Relative expression profile of related genes which corresponded to DAPs in lodicules of YM18 (gray column) and *ZK001* (black column).

A to I: relative expression profile of carbohydrate-related genes in lodicules of YM18 and *ZK001*. **J to K:** relative expression profile of calcium ion binding-related genes in lodicules of YM18 and *ZK001*. The results presented are the means of three independent experiments. Error bars, s.d. Columns marked with different lowercase letter indicate difference in means of YM18 (gray lowercase) and *ZK001* (black lowercase) using the one-way ANOVA LSD analysis of PASW Statistics software. The asterisk indicates the difference between YM18 and *ZK001* at WAS, GAS, YAS and AS, respectively. The data were further analyzed using an ANOVA at a 95% confidence level following Duncan's test (SPSS 18.0, IBM, Somers, NY, USA). The level of significance was set at $P \le 0.05$ or $P \le 0.001$.
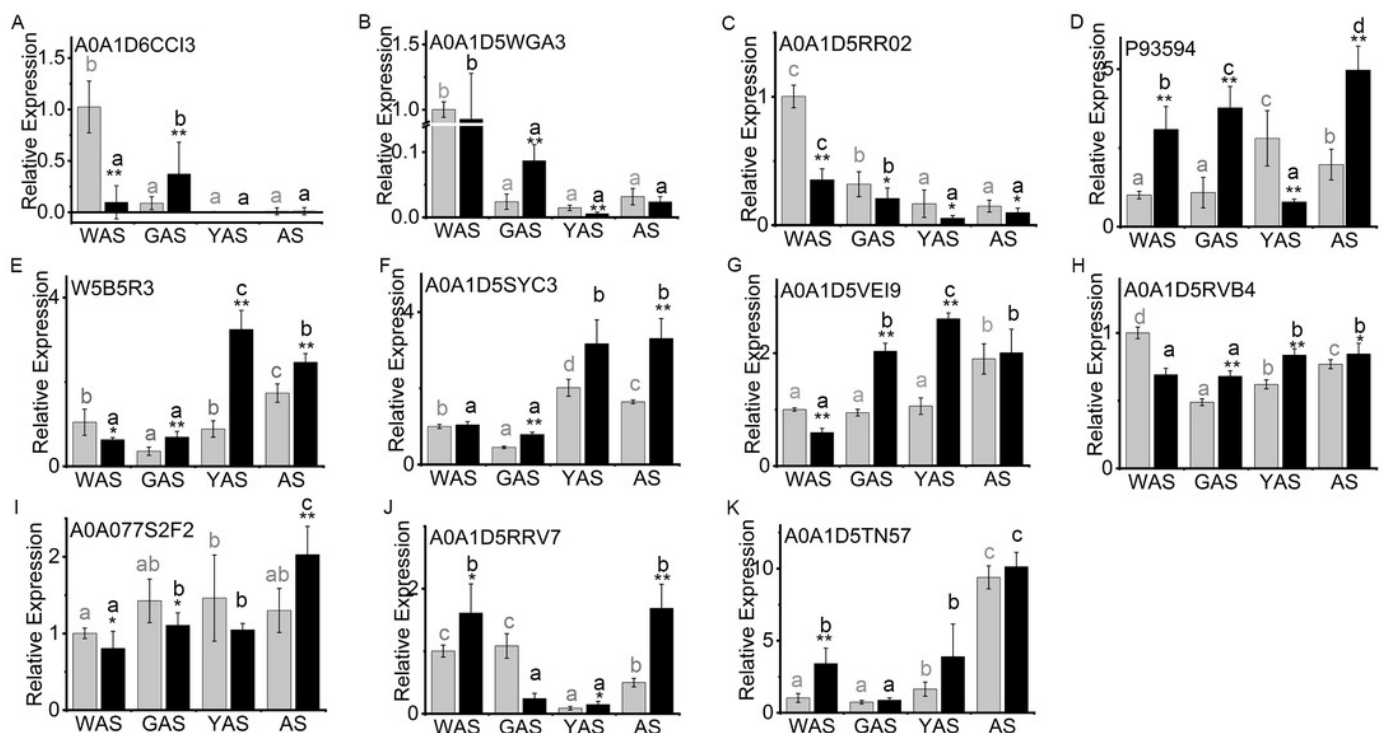
Figure 6

An overview of the pathway for proteome metabolic changes between YM18 and *ZK001*.

A: A0A1D6CCI3 (bidirectional sugar transporter SWEET); **B**: A0A1D5SYC3 (cellular glucose homeostasis-related proteins); **C**: A0A1D5RVB4 (cellular glucose homeostasis-related proteins); **D**: A0A1D5VEI9 (cellular glucose homeostasis-related proteins); **E**: A0A077S2F2 (beta-glucosidase activity-related protein); **F**: W5B5R3 (sucrose synthase); **G**: A0A1D5RR02 (beta-amylase); **H**: A0A1D5RRV7 (annexin); **I**: A0A1D5TN57 (calcium ion binding-related protein); **J**: A0A1D5WGA3 (nutrient reservoir-related protein); **K**: P93594 (beta-amylase).
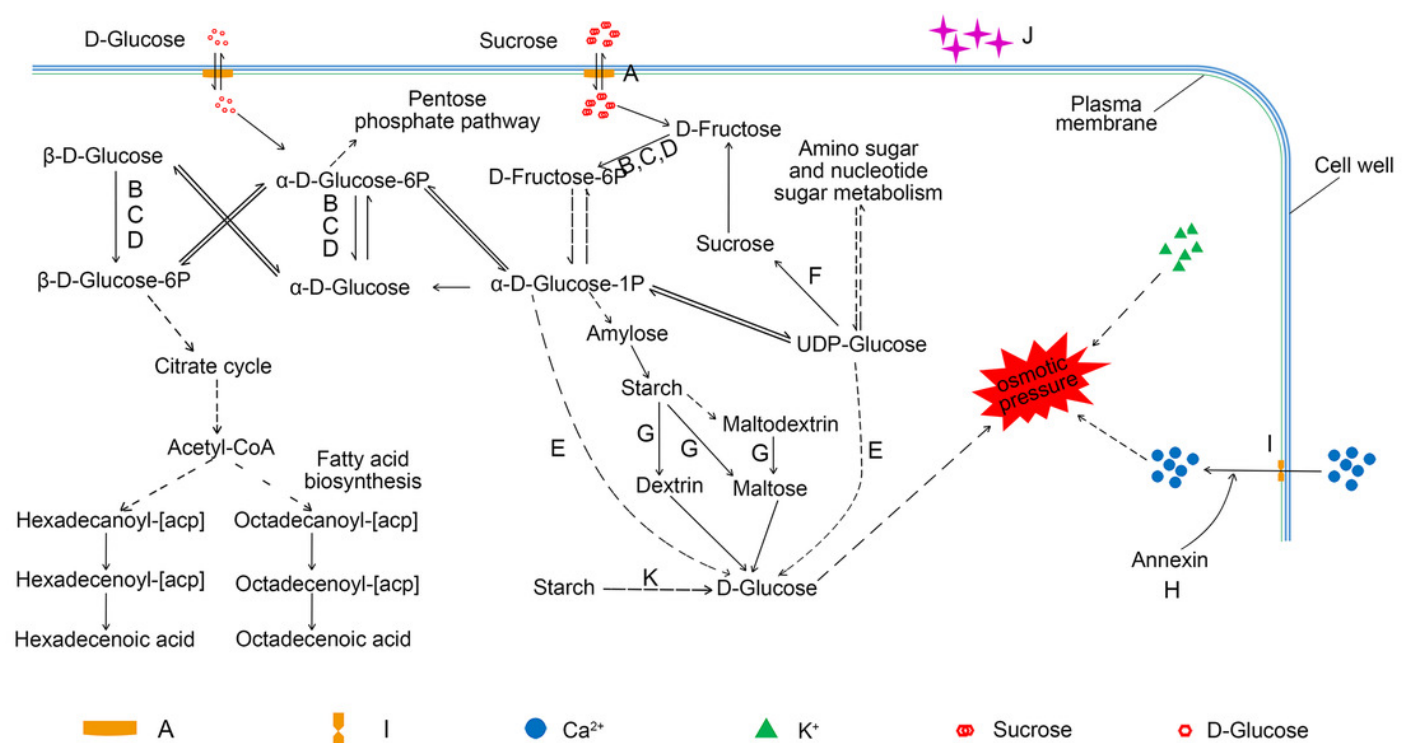
Comparison of diseased spikelets rate by *Fusarium* head blight in 2013-2014 and 2014-2015 in four varieties.

1 **Table 1**. Comparison of diseased spikelets rate by *Fusarium* head blight in 2013-2014 and 2014-2015 in four
2 varieties.

Variety	Diseased spikelets rate[a] (%)	
	2013-2014	2014-2015
SM3	7.03 ± 2.23	8.61 ± 3.40
ZK001	9.39 ± 3.31	17.60 ± 3.60
YM18	15.20 ± 2.46	35.16 ± 3.71
AK58	20.41 ± 6.76	38.12 ± 6.13

3 a: Diseased spikelets rate=the number of infected spikelets/total number of spikelets×100%. The results presented
4 are the means of three independent experiments. Error bars, s.d.

The number of differentially abundant proteins (DAPs) at four flower development stages.

(0.667 < FC < 1.5, corrected *P*–value < 0.01)

1 **Table 2**. The number of differentially abundant proteins (DAPs) at four flower development stages. (0.667 < FC <

2 1.5, corrected P–value < 0.01, PSMs ⩾ 2)

Groups	Total	Corrected P–value < 0.01		
		Increasing-DAPs	Decreasing-DAPs	Total DAPs
Group 1	4188	7	9	16
Group 2	4188	9	38	47
Group 3	4189	1	1	2
Group 4	4189	0	0	0
Group 5	4188	0	11	11
Group 6	4188	27	97	124
Group 7	4188	31	74	105
Group 8	4188	4	11	15
Group 9	4188	123	175	298
Group 10	4188	94	94	188

3 Note: Group 1: *ZK001*-WAS vs YM18-WAS, Group 2: *ZK001*-GAS vs YM18-GAS, Group 3:

4 *ZK001*-YAS vs YM18-YAS, Group 4: *ZK001*-AS vs YM18-AS, Group 5: YM18-WAS vs YM18-

5 GAS, Group 6: YM18-WAS vs YM18-YAS, Group 7: YM18-WAS vs YM18-AS, Group 8:

6 *ZK001*-WAS vs *ZK001*-GAS, Group 9: *ZK001*-WAS vs *ZK001*-YAS, and Group 10: *ZK001*-WAS

7 vs *ZK001*-AS.